Journal of Sound and Vibration (2000) **232**(4), 669–694
doi:10.1006/jsvi.1999.2773, available online at http://www.idealibrary.com on IDEAL®

ENERGY CONFINEMENT IN IMPERFECT PERIODIC SYSTEMS

D. YAP AND D. CEBON

University Engineering Department, Cambridge CB2 1PZ, England

(*Received* 21 *November* 1997, *and in final form* 13 *September* 1999)

The energy fraction Δ_{avg} is developed as a measure of energy confinement in periodic systems of finite extent. Based on the response of a system to uniform broadband forcing, Δ_{avg} is experimentally measurable but can be expensive to calculate. It is shown that a norm of the eigenvector matrix Δ'_{avg} is a good approximation for Δ_{avg} when damping is light. Δ'_{avg} is almost three orders of magnitude faster to calculate than Δ_{avg}, which makes detailed Monte Carlo studies of imperfections practical. One-dimensional linear-chain and cyclic systems of a range of sizes are studied. In line with previous research, it is found that a periodic system's propensity to confine energy increases with system size. It is also found that cyclic systems are less likely to suffer energy confinement than (otherwise equivalent) linear-chain systems.

1. INTRODUCTION

Many structures are composed of nominally identical substructures arranged in a linear chain or in a cyclic chain. Examples of such structures are: skin-stringer assemblies used in aircraft fuselages, multi-bay truss structures like the proposed international space station, and turbine blade assemblies. It is common to model such structures as perfectly periodic systems composed of identical subsystems because such models lead to straightforward predictions of vibration behaviour. However, even small imperfections can cause such predictions to be qualitatively incorrect. This paper is concerned with the vibration of *imperfect* periodic systems of finite extent, and specifically with quantifying their propensity to confine energy rather than allowing it to spread throughout the system. This behaviour is usually known as *localization*, a carryover from solid-state physics where it was first predicted for electrical conduction in disordered solids.

Localization theory was developed for infinite systems but many engineering systems are composed of too few subsystems for this to be a valid assumption, so straightforward application of results from solid-state physics to structural dynamic problems is often not possible. Nevertheless, energy confinement in finite systems has been predicted and experimentally observed.

In structural dynamics, many researchers have conducted deterministic analyses of the *free vibration* modes of disordered one-dimensional structures [1–6]. Others have conducted statistical analyses by studying the forced response of linear-chain systems to *single frequency* excitation applied to a single subsystem. This is justified by the argument of Matsuda and Ishii [7] that at a given frequency the localized mode shapes feature the same (exponential) spatial decay as the forced response. Since localization leads to exponential decay of the vibration modes, it is usually quantified in terms of the localization factor γ,

0022-460X/00/190669 + 26 $35.00/0

which is defined such that (on average) the mode shapes or vibration amplitudes (in the case of forced response) decay by $e^{-\gamma N}$ over N subsystems.

In the past decade, a useful distinction has developed between strong localization and weak localization. In general terms, strong localization occurs when subsystem disorder is high relative to coupling between subsystems. In real structures, unintentional disorder rarely exceeds 3–4%, so strong localization is usually associated with weak coupling. If the coupling is strong, only weak localization can occur. This happens if the ratio of disorder to coupling strength is low but the system in question is very large so that localization effects are inevitable. It is this latter category that is most akin to the phenomenon as it arises in solid-state physics, so it is not surprising that much of localization theory in the structural dynamics context is couched in language appropriate for the study of weak localization in infinite systems. In particular, travelling wave analyses are often applied which neglect the effect of boundary conditions (see, e.g., reference [8]).

Pierre [9] showed that weak localization is not of practical concern in many engineering structures. He gave an example of a weakly localized system in which 555 sites (subsystems) were needed for the vibration amplitude to decay by a factor of two. Not only would an engineering structure comprised of these many substructures be uncommon, it is likely that damping effects would be much more significant in causing decay of vibration, making weak localization effects imperceptible. Bouzit and Pierre [10] also found that the accuracy of a travelling wave approach deteriorates for large γ, in spite of the fact that for large γ boundary effects would diminish in significance. While they were unable to give an explanation for this, it was a consistent observation in their simulations. They concluded that a travelling wave analysis does not handle strong localization well, and that a modal approach should be used instead.

For finite systems significant localization must manifest itself within the length of the system, so any localization in finite systems must fall into the "strong" regime. In particular, the effect must be observable in the normal modes of the system, hence the term "normal-mode localization" implies strong localization. Furthermore, γ is not an ideal measure of localization in finite systems because of reflections from the boundaries. In light of this, several measures have arisen to quantify localization in finite systems. These range in sophistication from *ad hoc* comparisons of amplitude ratios of individual modes [2, 11] to norms of the eigenvector matrix [6, 12, 13]. None of these, however, has gained widespread use, and γ is still the dominant measure of localization even for finite systems.

The energy fraction developed in this paper is a direct measure of energy confinement in finite systems, which can be measured experimentally, as well as, predicted theoretically. For light damping, it is shown that the energy fraction can be approximated as a norm of the eigenvector matrix, making it an economic measure of localization in finite systems. The theory presented in this paper is developed for single-degree-of-freedom systems. However, this is not a practical limitation. Structures that are prone to localization generally have spectral filtering behaviour featuring distinct pass-bands and stop-bands. Each pass-band corresponds to one type of subsystem motion, that is, one degree of freedom in multi-degree-of-freedom systems. In effect, each degree of freedom can be modelled as a separate system.

The energy fraction was used successfully to predict localization behaviour in a 12-rib wrap-rib structure [14]. The experimental results of that study will be the subject of a subsequent paper.

1.1. MODE LOCALIZATION VERSUS ENERGY CONFINEMENT

There are two practical reasons to be concerned with localization phenomena. The first has to do with distortion of the normal modes. This is relevant in control of structural

dynamics (for example) where the presence of localized modes can invalidate control schemes that are based on the extended modes of a perfect structure. This is particularly important for future large space structures [3, 4, 15, 16]. In such applications it is necessary to calculate the normal modes of a disordered structure during the design phase, and assess whether localization is likely to be significant (indeed, it may be desirable). The complexity and considerable expense of predicting responses (in numerical simulation) can be avoided.

On the other hand, many engineering applications are concerned with the confinement of (vibration) energy in the proximity of where it is input; thus, localization is also a "response phenomenon". In this sense, localization occurs when extended disorder in a nominally periodic system causes *all* the normal modes to be confined to local regions. It is not enough for some modes to be localized, since significant energy transport can still occur through the remaining extended modes (a fact observed by Friedmann *et al.* [13]). Direct measures of energy confinement should therefore be based on the response of a system (sum of the modal responses) to a specific excitation. Frequency response functions are an obvious way to compare perfect and imperfect systems since their construction entails a modal sum. However, such calculations are computationally expensive to the extent that even with modern engineering workstations, detailed Monte Carlo studies of large systems may still be prohibitive.

As an alternative, Pierre [9] (after reference [17, 21]) derived an exact expression for $\gamma(\omega)$ in finite systems to single frequency forcing applied to one end of a linear chain. The solution does not require the response to be calculated; indeed, only the natural frequencies of the disordered system need to be found. However, it does not hold if the forcing frequency ω is a natural frequency of the system and, in any case, it is only applicable to linear-chain systems. The measure of energy confinement proposed in this paper is applicable to all types to systems: cyclic as well as linear chain, and also to systems of higher dimensionality.

1.2. ENERGY CONFINEMENT DUE TO DAMPING

As well as being a response phenomenon, energy confinement in disordered periodic systems is also a "resonance phenomenon". Since most of the energy flow in a periodic structure occurs in its pass-bands (indeed, energy cannot propagate long distances outside of the pass-bands), it is the degradation of energy transport within the pass-band of the ordered system that accounts for the largest difference in behaviour between ordered and disordered systems. This implies that damping is important in determining system behaviour. From the first, Hodges [22] stated that damping can overwhelm localization effects. In large systems (as in solid-state physics) it is natural to talk of a "localization length-scale", which is roughly the length of the region over which the amplitude of a localized mode is large [23–25]. Pierre [9] uses the reciprocal of the localization factor γ^{-1} as a measure of this localization length. If dissipation due to damping significantly attenuates vibration before this length is reached, it can be said that damping has overwhelmed the localization effect.

In finite systems, the level of damping necessary to overwhelm localization effects is that which would make a system non-reverberant (in reverberant systems propagating waves are reflected many times by the boundaries before being dissipated). For one-dimensional systems, the degree of modal overlap directly determines whether a system is reverberant or not [23]. Damping will dominate localization effects if the modal half-power bandwidth is significant compared to the frequency separation of the modes [20]—that is, when it is not possible to distinguish the individual modes in a pass-band. In structural dynamics, however, highly reverberant systems are often encounted. In such systems, damping is of

secondary importance, and perhaps for this reason most studies of localization phenomenon have not considered damping effects systematically.

Of the studies that have considered damping effects (among them references [13, 18, 26, 27], only two have compared energy confinement due to damping and that due to disorder over a sufficiently broad range of parameters to have arrived at general conclusions. Castanier and Pierre [28] and then Langley [29] found that the conditions that favour strong localization due to disorder also led to high spatial decay (confinement of vibration) due to damping. Langley, in particular, showed that the exponential decay rate due to damping is approximately inversely proportional to the pass-band width. That is, narrower pass-bands (which are consequence of weaker coupling) lead to greater energy confinement due to damping. This is true also of energy confinement due to disorder. For fairly modest levels of damping, Langley found that energy confinement due to damping was comparable in magnitude to that due to disorder. Castanier and Pierre [28] concluded that with strong coupling, damping effects dominate.

1.3. ENERGY CONFINEMENT IN TERMS OF ENERGY FRACTION

The prevailing measure of localization γ is a measure of spatial decay in the modes, and also of the spatial response distribution of imperfect systems to forcing at a *single frequency*. The view of imperfect periodic systems developed here focuses on the response to *broadband* forcing, which Hodges and Woodhouse [19] found to differ significantly from the response to single frequency forcing. In their simulations of broadband forcing they found that the decay away from the excited subsystem was not accurately exponential and the decay rate with distance was substantially less than that of the single frequency response. This might be expected since broadband forcing would result in excitation of more modes than single frequency forcing, thereby generating more 'paths' for energy transport.

There are few studies that have considered the response to broadband forcing [19, 20, 29], yet it is undeniable that such forcing is of practical importance. Since the effect of imperfections is greatest with narrow pass-bands, it is likely that a realistic force spectrum will have significant magnitude across a system's pass-band(s). In any case, this would certainly be true for shock loadings or if a system was subjected to random noise. Indeed, it seems reasonable that in applications where energy confinement is an issue, broadband forcing is more relevant than forcing at a single frequency.

The aspect of system behaviour that is studied here is spatial energy confinement. In particular, for a periodic system subjected to broadband forcing on one of its subsystems, it is desired to find the fraction of the total input energy that remains in the excited subsystem as a function of the overall imperfection in the system. This is a direct measure of energy isolation. Clearly, this quantity can be calculated from the response of *all* the subsystems to the applied force, and this is how the energy fraction is defined. For light damping ($\zeta \ll 1$), it is shown that an excellent approximation for the energy fraction can be obtained directly as a norm of the eigenvector matrix. Indeed, this norm is the exact solution for zero damping and represents the energy confinement due solely to imperfections.

Subsequent to the development of the theory, one-dimensional linear chain and cyclic systems are investigated in detail. A comparison is made between the energy confinement behaviour of these two types of systems, with particular attention paid to the effect of system size. It is commonly known that larger systems are more susceptible to localization, but, to the best of the author's knowledge, this effect has not been extensively studied.

2. ENERGY FRACTION AS A MEASURE OF LOCALIZATION

Many studies of localization in linear-chain systems (see, e.g., references [9, 10, 19]) have examined localization effects directly by exciting one end of a finite linear chain and calculating or measuring the response of the subsystems away from the excitation. The localization factor γ is then calculated from an ensemble average of the logarithm of the response† over many configurations of the system in question. This approach is obvious for a linear-chain system, but is not suitable for a cyclic system which does not possess *ends*. If this technique is modified by measuring the responses due to exciting *every* subsystem and averaging the results, the outcomes is a measure that has the advantage that it could be applied equally to linear-chain and cyclic systems, and indeed, to systems of higher dimensionality. At first sight, this measure seems to be N times more expensive to calculate, but it should be noted that this one measure contains as much statistical information as N configurations where only the end subsystem is excited. Such a measure is developed here and the remainder of this section is concerned with finding an economical method for calculating it.

Consider a system composed of N coupled single degree of freedom (d.o.f.) oscillators (subsystems) with light damping, such that the system is reverberant. Assuming that the eigenstructure for a particular configuration of imperfections is available, the response of the jth subsystem Y_{ij} to sinusoidal input $X_i e^{i\omega t}$ on the ith subsystem at a frequency ω is given by the usual formula [31]

$$H_{ij} = \frac{Y_{ij}}{X_{ij}} = \sum_{k=1}^{N} \frac{\phi_{ki}\phi_{kj}}{\omega_k^2 + 2i\zeta_k\omega_k\omega - \omega^2}, \tag{1}$$

where ϕ are the eigenvectors, ω_k are the eigenvalues, and ζ_k are the modal damping ratios. If a broadband forcing with spectral density $S_{x_i}(\omega)$ is applied to the ith subsystem, then the mean-square response in the pass-band is given by

$$E_{ij} = \int_{\omega_a}^{\omega_b} |H_{ij}|^2 S_{x_i}(\omega)\, d\omega. \tag{2}$$

where the frequency range ω_a to ω_b encompasses all the ω_k. The potential energy in the pass-band is proportional to E_{ij}, and it is assumed that the scaling factor is the same for all subsystems (i.e., the subsystems are nominally identical). As we are concerned with energy ratios, no generality is lost by using a scaling factor of "1".

The total energy in the system is the sum of the energies in all of the subsystems:‡

$$E_{tot} = \sum_{j=1}^{N} E_{ij}. \tag{3}$$

The energy fraction Δ_i is defined as the ratio of the energy that remains in the excited (ith) subsystem to the total energy in the system,

$$\Delta_i = \frac{E_{ii}}{E_{tot}}. \tag{4}$$

†See Hodges and Woodhouse [19, 30] for a discussion on averaging in γ calculations.

‡The energy in the coupling elements, which in practice may not be small, is nonetheless ignored.

Note, if $S_{x_i}(\omega)$ is uniform across $\omega_a \leqslant \omega \leqslant \omega_b$, it cancels out of the numerator and the denominator of equation (4), so that Δ_i is independent of the magnitude of the forcing. However, the forcing must not be so great that the system no longer behaves linearly. Repeating this calculation for all the subsystems (over index i) and taking the average gives the required result,

$$\Delta_{avg} = \frac{1}{N} \sum_{i=1}^{N} \Delta_i. \tag{5}$$

The greater Δ_{avg}, the greater the degree of energy localization. For example, if $\Delta_{avg} = \frac{1}{2}$ then (on average) half the energy input to a subsystem remains in that subsystem while the other half is distributed among the remaining $N-1$ subsystems. For comparison, if $\Delta_{avg} = \frac{3}{4}$, three-quarters of the input energy remains in the excited subsystem, indicating a greater degree of energy localization.

There are various ways to calculate or measure energy other than the definition used here. Each method will yield slightly different values of Δ_{avg}. However, since Δ_{avg} is a ratio, it is fairly robust and as long as the discrepancies between the energy calculation or measurement methods are consistent, the results should be very similar. Thus, the definition of Δ_{avg} can be relaxed to admit other measures of energy. For example, mobility (velocity) could be used as the frequency response function (equation (1)) rather than the receptance (displacement), or hysteretic damping could be assumed rather than viscous damping. Indeed, there are other ways to calculate energy altogether. For instance, Langley presented an efficient travelling wave analysis of average subsystem kinetic energy in reference [29]. In experimental studies, subsystem energy could be calculated in the time domain (by integrating over many cycles) or in the frequency domain, by summing the (squared) response spectrum over the pass-band of the system. The latter method was used in an experimental study of a radial, string-beam structure [14]. Attention is turned now to a direct measure of energy fraction that does not require calculation of the response at all.

3. CALCULATING Δ_{avg} FROM THE EIGENVECTORS

Calculating Δ_{avg} from equations (1)–(5) is computationally expensive, especially if a Monte Carlo study must be performed. In this section an expedient method of approximating Δ_{avg} directly from the eigenvectors is derived. The approximation depends on a few assumptions, which are described in context, but these assumptions are not too restrictive and the conditions under which they fail are investigated subsequently.

The pivotal requirement in the derivation is that the eigenvector matrix be orthogonal so that the sum of the squared elements of each of the columns and each of the rows is equal to 1. This requires the eigenvectors to be length normalized. To accommodate this scaling it is necessary to assume that the subsystems are nominally identical; this assumption poses no difficulty since it is fundamental to the definition of a periodic system.

For clarity of notation, the derivation is presented for a system of size $N = 3$ but the results are generally applicable. To begin, it is assumed that the eigenvectors of the system are the columns of the following matrix:

$$\mathbf{\Phi} = \begin{bmatrix} \phi_{11} & \phi_{12} & \phi_{13} \\ \phi_{21} & \phi_{22} & \phi_{23} \\ \phi_{31} & \phi_{32} & \phi_{33} \end{bmatrix}, \tag{6}$$

where the rows of $\mathbf{\Phi}$ correspond to the system co-ordinates, one per subsystem. It is also assumed that the corresponding eigenvalues are ω_1, ω_2, and ω_3.

The response of the system to a sinusoidal excitation applied to the first subsystem is (from equation (1))

$$Y_{11} = (\phi_{11}\phi_{11}f_1 + \phi_{21}\phi_{21}f_2 + \phi_{31}\phi_{31}f_3)X_1, \tag{7}$$

$$Y_{12} = (\phi_{11}\phi_{12}f_1 + \phi_{21}\phi_{22}f_2 + \phi_{31}\phi_{32}f_3)X_1, \tag{8}$$

$$Y_{13} = (\phi_{11}\phi_{13}f_1 + \phi_{21}\phi_{23}f_2 + \phi_{31}\phi_{33}f_3)X_1, \tag{9}$$

where

$$f_k(\zeta_k, \omega_k, \omega) = \frac{1}{\omega_k^2 + 2\mathrm{i}\zeta_k\omega_k\omega - \omega^2}, \quad k = 1, 2, 3. \tag{10}$$

From equation (2) the energy in the first subsystem when subjected to *uniform* broadband excitation $S_{x_1}(\omega)$ is

$$E_{11} = \int_{\omega_a}^{\omega_b} |\phi_{11}\phi_{11}f_1 + \phi_{21}\phi_{21}f_2 + \phi_{31}\phi_{31}f_3|^2 S_{x_1}(\omega)\,\mathrm{d}\omega \tag{11}$$

$$\begin{aligned} &= S_r \int_{\omega_a}^{\omega_b} (\phi_{11}^2\phi_{11}^2 |f_1|^2 + \phi_{11}^2\phi_{21}^2 |f_1||f_2| + \phi_{11}^2\phi_{31}^2 |f_1||f_3| \\ &\quad + \phi_{21}^2\phi_{11}^2 |f_2||f_1| + \phi_{21}^2\phi_{21}^2 |f_2|^2 + \phi_{21}^2\phi_{31}^2 |f_2||f_3| \\ &\quad + \phi_{31}^2\phi_{11}^2 |f_3||f_1| + \phi_{31}^2\phi_{21}^2 |f_3||f_2| + \phi_{31}^2\phi_{31}^2 |f_3|^2)\,\mathrm{d}\omega, \end{aligned} \tag{12}$$

where $S_r = S_{x_1}(\omega_a) = S_{x_1}(\omega_b)$, since $\omega_a \approx \omega_b$ and $S_{x_1}(\omega)$ is assumed to be only varying slowly with frequency (if at all). Similar expressions can be derived for E_{12} and E_{13}. To simplify equation (12) two assumptions are made. First, it is assumed that the modal responses do not overlap significantly in frequency. That is, in the frequency range where f_1 is large, f_2 and f_3 are assumed to be negligible, and similarly for f_2 and f_3 in the frequency ranges where they dominate. This require $\zeta_k \ll 1$ since the errors will increase with ζ_k. This assumption allows the cross-terms of E_{11} (which feature products $|f_p||f_q|$, $p \neq q$) to be ignored. Second, it is assumed that

$$F = \int_{\omega_a}^{\omega_b} |f_1|^2\,\mathrm{d}\omega = \int_{\omega_a}^{\omega_b} |f_2|^2\,\mathrm{d}\omega = \int_{\omega_a}^{\omega_b} |f_3|^2\,\mathrm{d}\omega, \tag{13}$$

which, in practice, amounts to the assumption that $\zeta_1 = \zeta_2 = \zeta_3 \ll 1$ and that the frequency-integrated modal responses are dominated by the responses close to the resonance frequencies so that the integrals are insensitive to the choice of ω_a and ω_b. With these two assumptions the energy in each of the subsystems is given by

$$E_{11} = (\phi_{11}^2\phi_{11}^2 + \phi_{21}^2\phi_{21}^2 + \phi_{31}^2\phi_{31}^2)F^2 S_r, \tag{14}$$

$$E_{12} = (\phi_{11}^2\phi_{12}^2 + \phi_{21}^2\phi_{22}^2 + \phi_{31}^2\phi_{32}^2)F^2 S_r, \tag{15}$$

$$E_{13} = (\phi_{11}^2\phi_{13}^2 + \phi_{21}^2\phi_{23}^2 + \phi_{31}^2\phi_{33}^2)F^2 S_r. \tag{16}$$

Then, from equation (4) the resulting energy fraction is

$$\Delta_1 = \frac{E_{11}}{E_{11} + E_{12} + E_{13}}. \tag{17}$$

When equations (14)–(16) are substituted into equation (17), $F^2 S_r$ cancels out leaving an expression solely in terms of elements of the eigenvectors. Performing the substitution and rearranging terms gives

$$\Delta_1 = \frac{\phi_{11}^2\phi_{11}^2 + \phi_{21}^2\phi_{21}^2 + \phi_{31}^2\phi_{31}^2}{\phi_{11}^2(\phi_{11}^2 + \phi_{12}^2 + \phi_{13}^2) + \phi_{21}^2(\phi_{21}^2 + \phi_{22}^2 + \phi_{23}^2) + \phi_{31}^2(\phi_{31}^2 + \phi_{32}^2 + \phi_{33}^2)}. \tag{18}$$

Due to orthogonality of $\mathbf{\Phi}$ each of the terms in parantheses in equation (18) is equal to 1 so

$$\Delta_1 = \frac{\phi_{11}^2\phi_{11}^2 + \phi_{21}^2\phi_{21}^2 + \phi_{31}^2\phi_{31}^2}{\phi_{11}^2 + \phi_{21}^2 + \phi_{31}^2}. \tag{19}$$

Again from orthogonality the denominator of equation (19) is also equal to 1 and the final result is

$$\Delta_1 = \phi_{11}^4 + \phi_{21}^4 + \phi_{31}^4. \tag{20}$$

Similar analyses for uniform broadband forcing applied to the second and third subsystems give

$$\Delta_2 = \phi_{12}^4 + \phi_{22}^4 + \phi_{32}^4 \tag{21}$$

and

$$\Delta_3 = \phi_{13}^4 + \phi_{23}^4 + \phi_{33}^4. \tag{22}$$

Referring to equations (5) and (6) it is evident that Δ_{avg} can be calculated by raising all of the components of the eigenvector matrix $\mathbf{\Phi}$ to the fourth power, summing the columns of the resultant matrix, and averaging these sums. Thus, under the assumptions previously stated, the energy fraction can be calculated as a norm of the length normalized eigenvector matrix, which is henceforth defined as

$$\Delta'_{avg} = \frac{1}{N}\sum_{j=1}^{N}\sum_{k=1}^{N}\phi_{jk}^4. \tag{23}$$

Clearly, Δ'_{avg} can be calculated for systems of any size N.

In the derivation of Δ'_{avg} no assumptions were made regarding the nature of the physical system apart from it being nominally periodic, having light damping ($\zeta_k \ll 1$, the same in all modes), and without significant modal overlap. Consequently, Δ'_{avg} is applicable to any system composed of coupled single-d.o.f. oscillators, whether the system is one-dimensional or even two- or three-dimensional. Furthermore, imperfections are allowed from any source; they may rise in the coupling ("off-diagonal" imperfection), and also in the subsystems' stiffnesses and masses ("diagonal" imperfection). However, in this paper thorough investigation of Δ'_{avg} is focused on one-dimensional, cyclic and linear-chain systems with nearest-neighbour coupling, and diagonal imperfections.

4. COMPARISON OF Δ_{avg} AND Δ'_{avg}

Δ'_{avg} is a measure of energy confinement due to imperfection in lightly damped systems. By comparison, Δ_{avg} is a measure of energy confinement due to imperfection *and* damping. In order to ascertain when the two measures are practically equivalent a parameter study of 2 d.o.f. systems is presented. This type of system is unique because all imperfections can be represented by a single parameter, which is simply the dissimilarity (in stiffnesses, say) between the two subsystems. By contrast, modelling larger systems requires the results to be averaged over an ensemble of imperfection configurations, necessitating an examination of the nature of these averages. This additional complexity is deferred until section 5.

It is straightforward to show that the eigenvalue problem associated with the 2 d.o.f. system shown in Figure 1 is [14]

$$[\mathbf{A}]\mathbf{\Phi} = \lambda\mathbf{\Phi}, \tag{24}$$

where

$$\lambda = \frac{m}{k_c}\omega^2, \tag{25}$$

$$[\mathbf{A}] = \begin{bmatrix} D & -1 \\ -1 & D+e \end{bmatrix}, \tag{26}$$

with $D = 2 + \rho$, $\rho = k_d/k_c$ and $e = \kappa/k_c$. The parameter values used were $m = 1$ kg and $k_c = 0{\cdot}1$ N/m. The subsystem stiffness k_d and the dissimilarity between the two subsystems κ were allowed to take values appropriate to achieve three different coupling ratios ($\rho = 10$, 100, 1000) and a broad range of imperfection ratios ($10^{-2} \leqslant e \leqslant 10^4$) respectively.

For each set of parameters the eigenvalue problem was solved and Δ'_{avg} was calculated using equation (23). For Δ_{avg}, which depends on damping as well as the eigenstructure, the damping ratio was introduced as an additional parameter; Δ_{avg} was calculated a for $10^{-5} \leqslant \zeta \leqslant 10^{-1}$.

4.1. RESULTS FOR 2 d.o.f. LINEAR-CHAIN SYSTEMS

The results of the parameter study are presented in three stages to show (1) the general behaviour of Δ_{avg} as the imperfection ratio is increased; (2) how damping increases energy confinement to the point that Δ'_{avg} cannot be taken as equivalent to Δ_{avg}; and finally (3) how the coupling ratio ρ influences the effect of damping by controlling the modal frequency spacing. To begin, consider the two graphs in Figure 2 where Δ_{avg} is plotted with Δ'_{avg} for $\rho = 100$ and the range of e previously noted. The top graph, Figure 2(a), shows the results

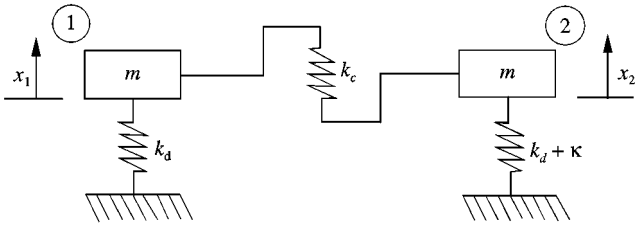

Figure 1. Two coupled oscillators.

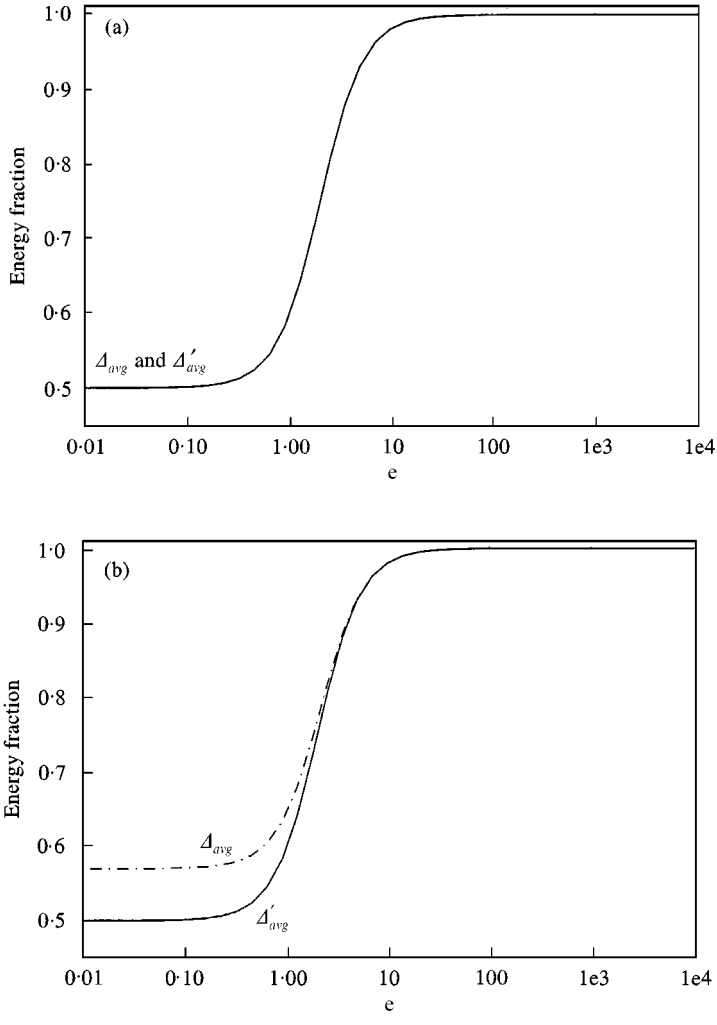

Figure 2. Variation of Δ_{avg} and Δ'_{avg} with imperfection for two damping ratios: (a) $\rho = 100$, $\zeta = 0{\cdot}0001$; (b) $\rho = 100$, $\zeta = 0{\cdot}002$. NB: Δ_{avg} and Δ'_{avg} overlap in (a).

for $\zeta = 0{\cdot}0001$ where it is evident that Δ_{avg} and Δ'_{avg} are identical. The general behaviour of the 2 d.o.f. system is as follows: with low values of e the energy fraction is $\frac{1}{2}$ indicating equal energy in the two subsystems. Not until $e = 0{\cdot}1$ is there an appreciable increase in energy fraction, and this value marks roughly the beginning of a transition region that spans three orders of magnitude of e. Where $e > 100$ near total energy confinement is achieved. Thus, the energy confinement shown in Figure 2(a) is due solely to dissimilarity between the two subsystems.

As discussed in Section 1, damping causes energy confinement in periodic systems similar to that due to imperfection. This is evident in Figure 2(b) where the damping ratio was increased to $\zeta = 0{\cdot}002$. Notice first that that Δ'_{avg} is the same in both figures since it is independent of ζ. By comparison, Δ_{avg} indicates a higher level of energy confinement for low values of e in Figure 2(b). This additional energy confinement is due to damping. Notice that the difference between Δ_{avg} and Δ'_{avg} decreases as e increases, which shows that the effect of imperfections dominate with large dissimilarity.

To illustrate the full relationship between energy confinement due to imperfection and that due to damping, Δ_{avg} and Δ'_{avg} are plotted in Figure 3 for the same range of e as in Figures 2, over a broad range of damping, $10^{-5} \leqslant \zeta \leqslant 10^{-1}$. Again, the Δ'_{avg} curve is the same for all values of ζ; the difference between Δ_{avg} and Δ'_{avg} is due solely to additional energy confinement caused by damping. The first notable observation is that if energy is totally confined ($\Delta_{avg} = \Delta'_{avg} = 1$) due to dissimilarity (where $e > 100$) then damping cannot, of course, increase energy confinement further. For $e < 100$, however, there is an increase in energy fraction with increasing ζ that is similar to that due to increasing e. Clearly, for high values of ζ, Δ'_{avg} is no longer equivalent to Δ_{avg}. However, for the given parameter range, Δ'_{avg} is a lower bound on Δ_{avg}. This is physically reasonable since damping should always increase energy confinement. The question that immediately arises is how much damping causes significant differences between Δ_{avg} and Δ'_{avg}?

In one-dimensional systems the level of modal overlap determines whether a system is reverberant or not. If a system is non-reverberant, clearly there must be significant energy confinement, so Δ_{avg} will be greater than Δ'_{avg} when ζ (which determines the bandwidth at resonance) is large such that there is significant modal overlap. However, modal overlap

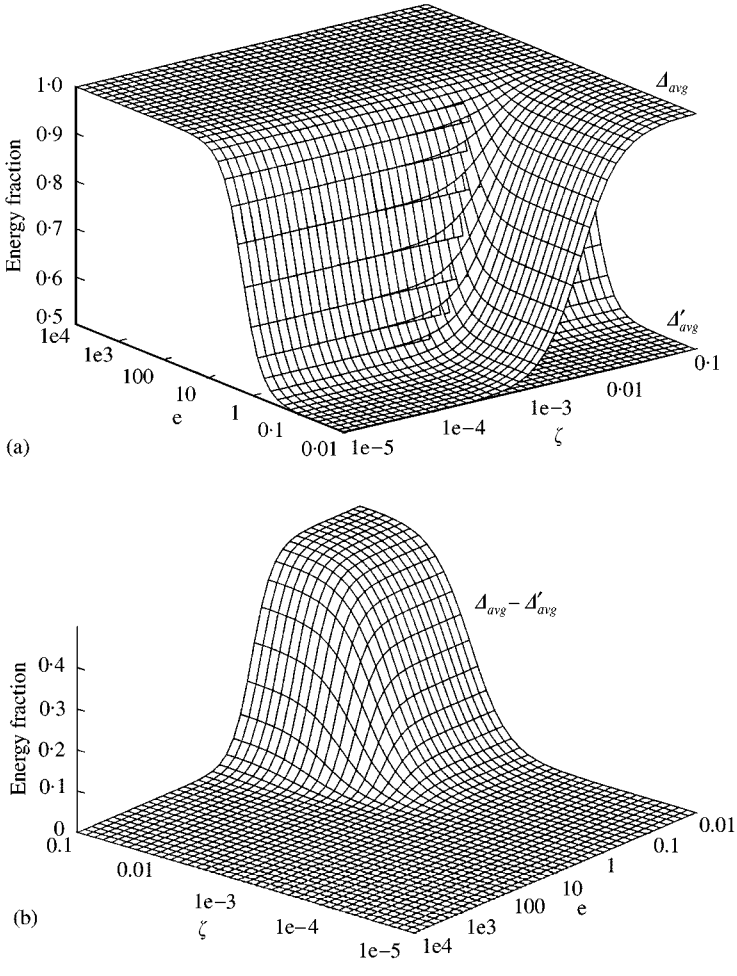

Figure 3. Variation of Δ_{avg} and Δ'_{avg} with imperfection *and* damping ratio as parameters.

also depends on the modal frequency spacing, which depends on the coupling ratio ρ. In particular, the pass-band width is inversely proportional to ρ [9, 29]. Larger values of ρ lead to narrower pass-bands and hence to smaller frequency spacings and greater modal overlap for a given ζ.

To see the correlation between energy confinement and modal overlap, compare the contour plot (Figure 4(a)) which shows the curve where $(\Delta_{avg} - \Delta'_{avg}) = 0{\cdot}1$ with the contour plot (Figure 4(b)) which shows the curve where the half-power bandwidths of the two modes overlap. These results are for $\rho = 100$, similar curves for $\rho = 10$ and 1000 were generated and the full set of results are shown in Figure 5. The exact relationship between Δ_{avg} and Δ'_{avg}

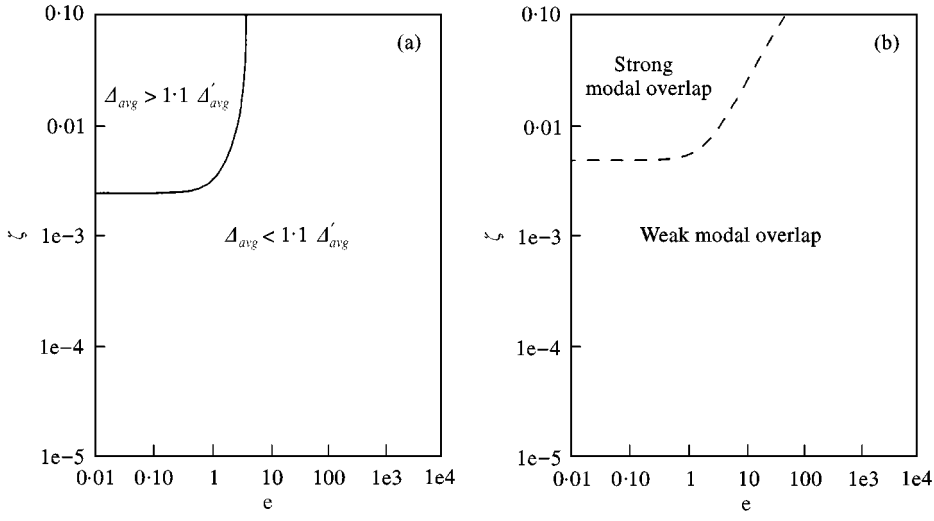

Figure 4. Energy fraction to modal overlap comparison for $\rho = 100$: (a) contour plot of $\Delta_{avg} - \Delta'_{avg} = 0{\cdot}1$; (b) contour plot of modal overlap. Dashed line indicates intersection of half-power bandwidths of the two modes.

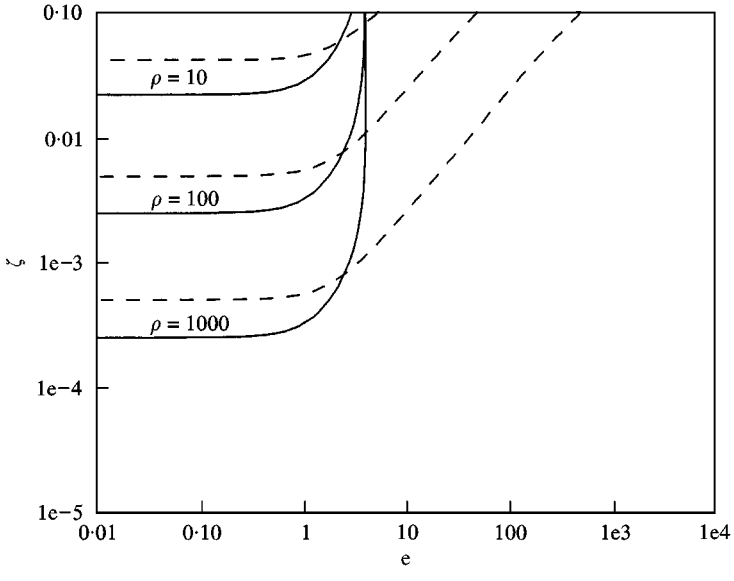

Figure 5. Energy fraction of modal overlap comparison for three coupling ratios (Figure 4 is a legend for this figure).

is not investigated further. However, Figure 5 confirms that there is a strong relationship between energy confinement due to damping and the degree of modal overlap, which, in turn, depends not only the damping ratio but also on the coupling ratio. In sum, when there is significant modal overlap, only Δ_{avg} gives an accurate account of the energy confinement in a periodic system. However, in the 2 d.o.f. system, Δ'_{avg} is a lower bound for Δ_{avg} and the difference between the two measures represents the energy confinement due to damping.

5. THE EFFECT OF SYSTEM SIZE

In this section the energy confinement behaviour of linear-chain systems is investigated as function of system size. As a preliminary step the mathematical model for generic one-dimensional systems is developed and the details of the calculations are presented. The statistical profile of the results are checked to ensure that they represent the behaviour of typical systems. The results show a definite size dependence: all other factors being equal, larger systems exhibit a greater propensity for energy confinement.

5.1. SIMULATIONS OF GENERIC SYSTEMS

In order to study systems larger than the 2 d.o.f. system considered so far it is necessary to perform numerical simulations. In particular, Δ_{avg} and Δ'_{avg} are calculated for generic systems of size N with diagonal imperfections in the $(N \times N)$ system matrices. The mathematical model of the 2 d.o.f. system can be extended by adapting $[\mathbf{A}]$ (equation (26)) for larger systems; hereafter referred to as $[\mathbf{A}_{C,N}]$ for cyclic systems or $[\mathbf{A}_{L,N}]$ for linear-chain systems. For example, the system matrix for the 12 d.o.f. cyclic system is expressed as

$$[\mathbf{A}_{C,12}] = \begin{bmatrix} D+\xi_1 & -1 & 0 & \cdots & 0 & -1 \\ -1 & D+\xi_2 & -1 & 0 & & 0 \\ 0 & -1 & \ddots & & & \vdots \\ \vdots & & & & & 0 \\ 0 & & & & \ddots & -1 \\ -1 & 0 & \cdots & 0 & -1 & D+\xi_{12} \end{bmatrix}. \tag{27}$$

This matrix represents all one-dimensional 12 d.o.f. cyclic systems with nearest-neighbour coupling. The only difference between $[\mathbf{A}_{L,12}]$ and $[\mathbf{A}_{C,12}]$ is the exclusion of the two anti-diagonal coupling terms (by replacing -1 with 0) at (1, 12) and (12, 1).

In this model, the diagonal imperfections ξ_i are given by

$$\xi_i = \Upsilon\psi_i, \quad i = 1, 2, \ldots, 12, \tag{28}$$

where ψ_i are random numbers uniformly distributed between 0 and 1, and the maximum imperfection ratio is

$$\Upsilon = \frac{\kappa_{max}}{k_c}. \tag{29}$$

κ_{max} is the maximum imperfection stiffness, and k_c is the coupling stiffness. The remaining variable in equation (27) is $D = 2 + \rho$, where $\rho = k_d/k_c$ is the ratio of the subsystems stiffness to the coupling stiffness.

To see when Υ is *the* governing parameter for energy confinement *due to imperfection*, note that changing k_d simply shifts the mean diagonal value of the system matrix. A well-known result from linear algebra (see, e.g., Joshi [32]) states that two matrices have the same eigenvectors if they commute. Thus, to prove that changing k_d does not affect the eigenvectors it is sufficient to show

$$[\mathbf{A}]([\mathbf{A}] + s[\mathbf{I}]) = ([\mathbf{A}] + s[\mathbf{I}])[\mathbf{A}], \tag{30}$$

where $[\mathbf{A}]$ is any matrix, $[\mathbf{I}]$ is a compatible identity matrix, and s is an arbitrary scalar. Carrying out the multiplications in equation (30) gives

$$[\mathbf{A}]^2 + [\mathbf{A}]s[\mathbf{I}] = [\mathbf{A}]^2 + s[\mathbf{I}][\mathbf{A}], \tag{31}$$

the two $[\mathbf{A}]^2$ terms in equation (31) cancel out, as does the scalar s, leaving the obvious result that $[\mathbf{A}][\mathbf{I}] = [\mathbf{A}][\mathbf{I}] = [\mathbf{A}]$. Therefore, since Δ'_{avg} is based solely on the eigenvectors it is unaffected by k_d. However, Δ_{avg} does depend on k_d since it directly affects the coupling ratio ρ which interacts with damping to produce energy confinement effects as described in the study of the 2 d.o.f. system.

5.2. DETAILS OF THE CALCULATIONS

Monte Carlo simulations were performed by averaging Δ_{avg} and Δ'_{avg} over many random configurations of $[\mathbf{A}_{C,N}]$ and $[\mathbf{A}_{L,N}]$ with $N = 3, 6, 12, 24, 48$, $\rho^{-1} = 0{\cdot}1$, and $\zeta = 0{\cdot}001$. The calculations were repeated over a wide range of imperfection to coupling ratios ($10^{-1} < \Upsilon < 10^4$) so that the entire transition from fully periodic to fully localized behaviour was included. The number of random configurations p that make up the averages varied from $p = 348$ for $N = 3$ to $p = 24$ for $N = 48$. In each case, the product $(N \times p) = 1152$, a number that was chosen primarily because of limitations in computer resources, but which also provided sufficiently *smooth* results that larger sample sets were not required.

The decision to use smaller sample sets as N increased was justified because the variances of Δ_{avg} and Δ'_{avg} both decrease as N increases. This behaviour is also true for the localization factor γ, as shown by Langley [33]. Whilst the energy fraction Δ_{avg} is not directly related to the localization factor γ, they both describe the same underlying phenomenon and it is reasonable that both measures should display similar statistical properties.

The major computational expense in the simulations resulted from the calculation of Δ_{avg}. Whereas, Δ'_{avg} required few additional computations beyond the calculation of a system's eigenvectors, the response functions that make up Δ_{avg} were very expensive to calculate. In practice, Δ_{avg} required approximately 800 times more floating-point operations to calculate than Δ'_{avg}. On a Sun Sparcstation 10, which can perform over 9 million floating-point operations per second, it took over a week to calculate Δ_{avg} for 24 random configurations of $N = 48$, but less than 15 min to calculate Δ'_{avg} for the same configurations! The calculations for $N = 48$ were the most expensive. Even though the number of random configurations was halved as system size was doubled, the time taken to complete the calculations increased by a factor between three and four times with each doubling of N. This significant saving in computational time was part of the impetus behind the development of Δ'_{avg}.

In the following sections results for the linear-chain systems are presented as a basis for general discussion of the behaviour of Δ_{avg} and Δ'_{avg}. The statistical profiles of the two measures are investigated to ensure that they predict the behaviour of typical systems

(rather than being unduly influenced by a few anomalous configurations). The subsequent introduction of comparable results for cyclic systems in section 6 then shows a significant difference between the energy confinement behaviour of the two types of systems. This difference is explained by examining the modes shapes of particular random configurations in section 7 which show how Δ_{avg} and Δ'_{avg} reflect dramatic changes in the systems' eigenstructures as the imperfection to coupling ratio increases.

5.3. STATISTICAL PROFILE OF Δ_{avg} AND Δ'_{avg}

In this section, typical ensembles from the Monte Carlo study are investigated in detail. In particular, it is necessary to confirm that the averages are a good indicator of *typical* system behaviour. As a first example, Δ'_{avg} was calculated for 256 random configurations of a 12 d.o.f. linear-chain system as the coupling k_c was decreased (Υ increasing). For this case, *all* the Δ'_{avg} values were retained—not just the averages. The results are shown as a shaded histogram in Figure 6, where darker shading indicates greater frequency of occurrence. Also plotted in Figure 6 are the mean value (solid line) and one standard deviation σ on either side of the mean (the two dashed lines bounding the mean). Cross-sections of Figure 6 for $\Upsilon = 1, 10, 100$ are shown in Figure 7. These figures show that for $\Upsilon < 100$, Δ'_{avg} is evenly distributed on either side of the mean value as typified by the results for $\Upsilon = 10$ shown in Figure 7. However, for $\Upsilon > 100$ the statistical profile features most of the Δ'_{avg} values clustered close to 1 with fewer configurations giving quite low values of Δ'_{avg}. This is most apparent in Figure 6. In sum, Δ'_{avg} is a good indicator of typical system behaviour for $\Upsilon < 100$, but for $\Upsilon > 100$ most configurations give values of Δ'_{avg} that are closer to 1.

The average values of Δ_{avg} and Δ'_{avg}, and the standard deviations σ of the two measures were also calculated in the Monte Carlo simulations for $N = 3, 12, 48$ (Figures 8(a)–(f)). It is

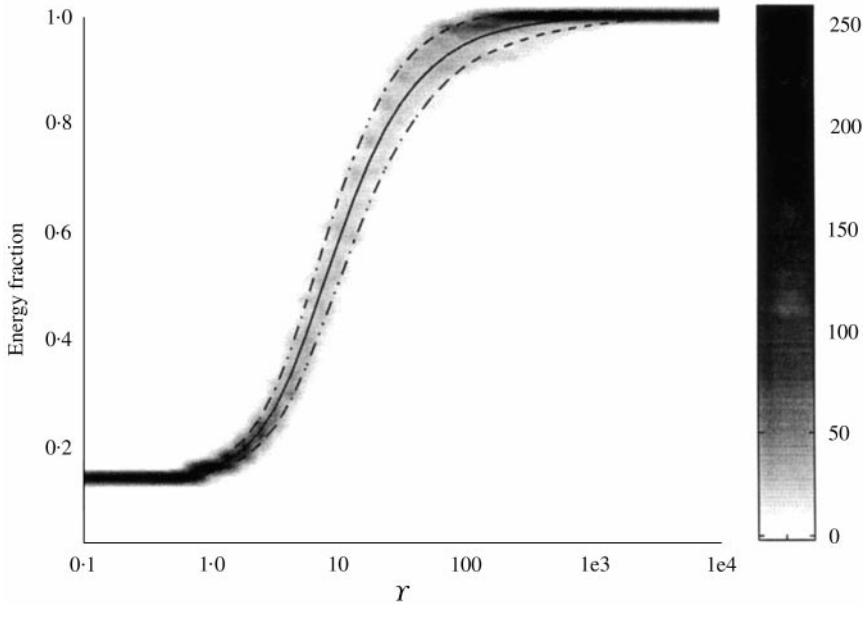

Figure 6. Shaded histogram of Δ'_{avg} for $N = 12$ taken over an ensemble of 256 random imperfection configurations. The mean and standard deviation $\pm\sigma$ are also shown.

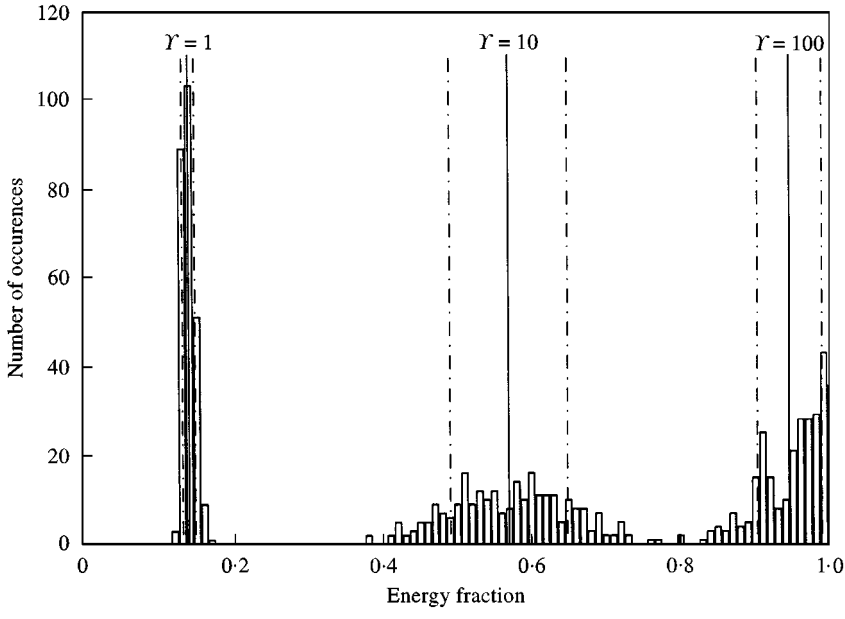

Figure 7. Cross-sections of the shaded histogram in Figure 6 for $\Upsilon = 1, 10, 100$. The mean values and σ are also shown as solid and dashed lines respectively.

evident that Δ_{avg} and Δ'_{avg} have very similar statistical profiles. This is expected since damping is not a major factor for the given parameter settings. Notice that $\Delta'_{avg} + \sigma$ (and $\Delta_{avg} + \sigma$) rises above 1 for certain regions of Υ. This is not because there were values of Δ_{avg} and Δ'_{avg} that were greater than 1—clearly this is impossible. Rather, this is due to the skewed distributions of Δ'_{avg} (and Δ_{avg}) as they approach 1, as noted above.

All three systems share common characteristics: there is no significant variation of Δ_{avg} or Δ'_{avg} from the mean for $\Upsilon < 1$ or for $\Upsilon > 10^3$, which corresponds to the two limiting cases of periodic behaviour and completely localized behaviour respectively. In the transition region there is a gradual increase in σ as Υ increases from 1 until a peak is reached around $\Upsilon = 10$, whereafter σ decreases to zero for $\Upsilon \gg 10^3$.

As noted in the previous discussion, the variance decreases with N, which justifies fewer members in the ensembles used to calculate the averages of larger systems. Scrutiny of the σ results showed that the *standard deviation* is roughly proportional to $1/\sqrt{N}$ for intermediate values of Υ. By contrast, the *variance* of the localization factor γ varies with $1/\sqrt{N}$ [33].

5.4. RESULTS FOR LINEAR-CHAIN SYSTEMS

The results for the linear-chain systems are presented in Figure 9, which shows the Monte Carlo averages of Δ_{avg} and Δ'_{avg} over the range of Υ and N previously mentioned with $\zeta = 0{\cdot}001$. In general, it is apparent that Δ_{avg} and Δ'_{avg} are very similar over the parameter range shown. At $\Upsilon = 0{\cdot}1$ both measures start off at an energy fraction somewhat greater than $1/N$. In the case of the 2 d.o.f. system, the energy fraction started out as $\frac{1}{2}$ with $\Upsilon = 0{\cdot}1$, indicating equal energy in the two subsystems. However, there is no reason to expect that the energy fraction should always have a value equal to $1/N$ at low values of Υ, and this does not always occur. Thus, even ordered systems do not distribute uniform broadband energy

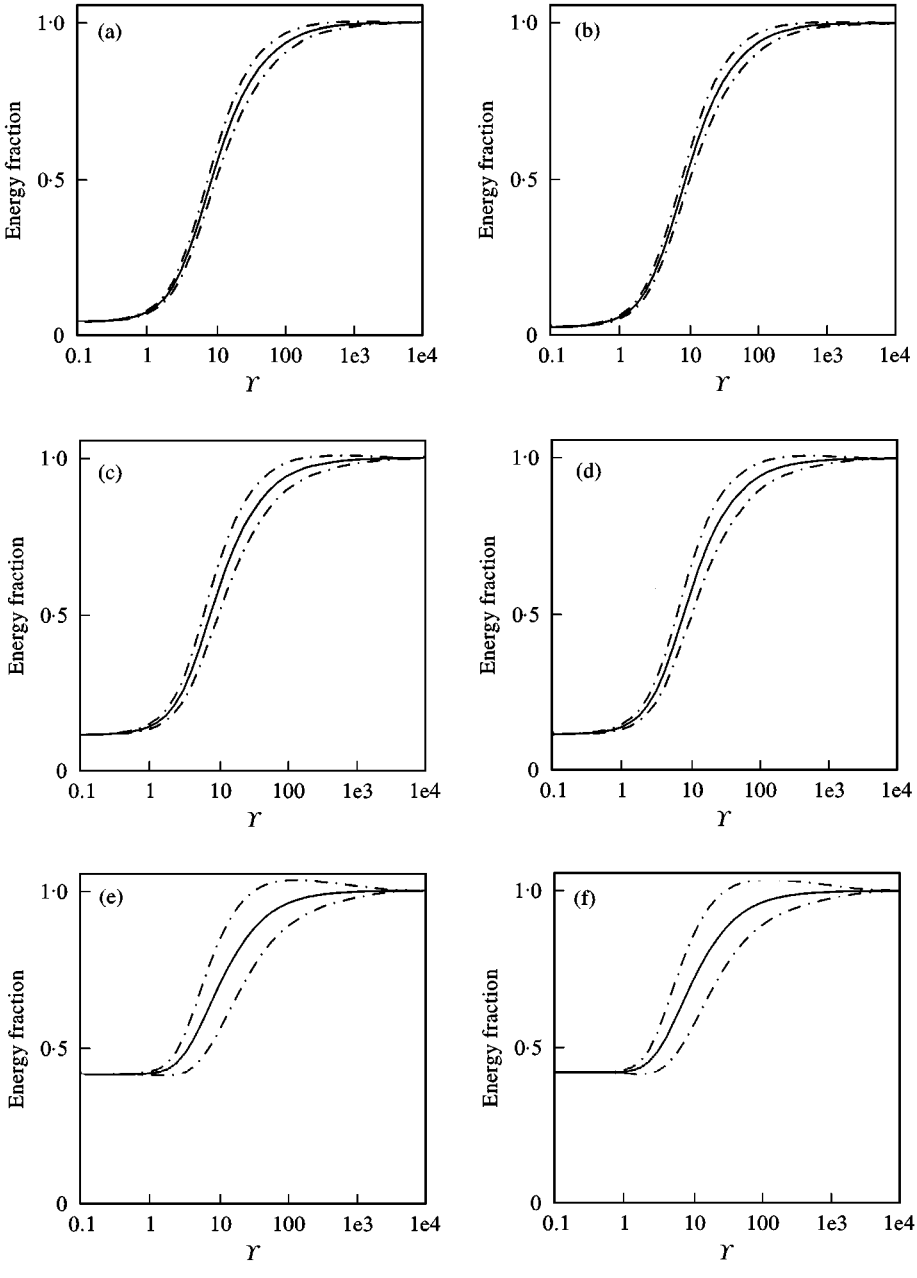

Figure 8. Mean and standard deviation of Δ_{avg} and Δ'_{avg} for linear-chain systems with $N = 3, 12, 48$: (a) Δ_{avg}, $N = 48$; (b) Δ'_{avg}, $N = 48$; (c) Δ_{avg}, $N = 12$; (d) Δ'_{avg}, $N = 12$; (e) Δ_{avg}, $N = 3$; (f) Δ'_{avg}, $N = 3$.

equally among all their constituent subsystems. However, imperfection always increases energy confinement, and as Υ increases, Δ_{avg} and Δ'_{avg} increase smoothly to 1, which corresponds to complete energy confinement.

For $N = 3$, 6, 12 the two measures are practically identical for engineering purposes. However, for $N = 24$, Δ_{avg} predicts a higher level of energy confinement than Δ'_{avg} at low values of Υ, and this discrepancy is more pronounced for $N = 48$. As for the 2 d.o.f. system,

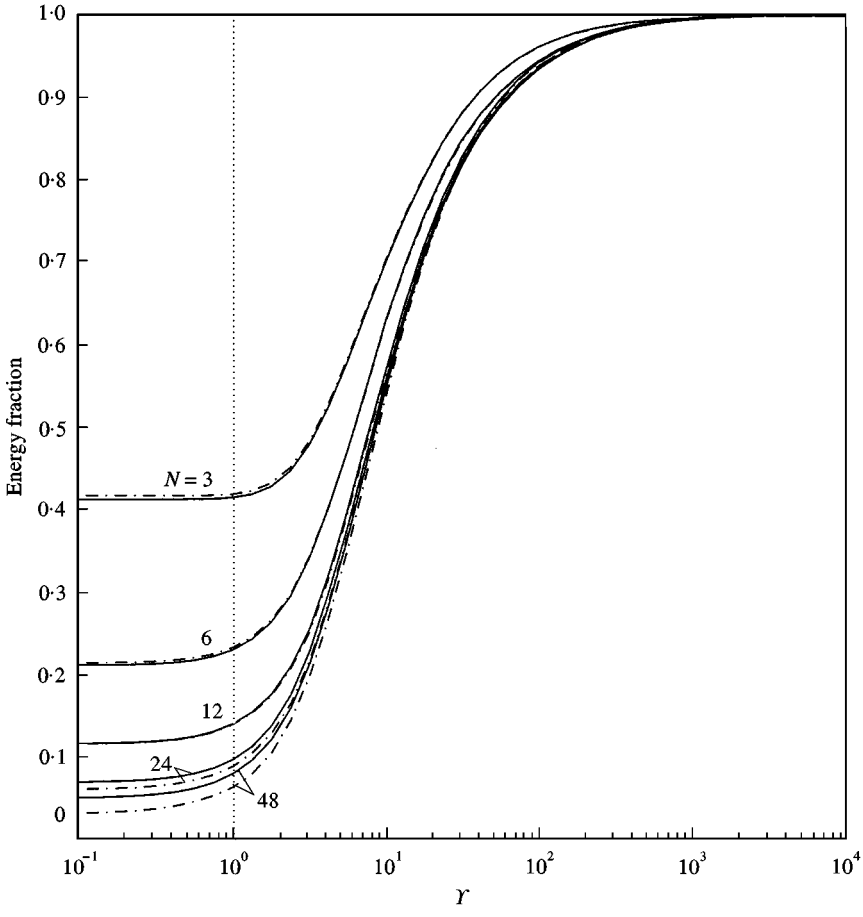

Figure 9. Δ_{avg} and Δ'_{avg} for linear-chain systems. $\rho^{-1} = 0{\cdot}1$, $\zeta = 0{\cdot}001$, $N = 3, 6, 12, 24, 48$. —— Δ_{avg}; –·–·– Δ'_{avg}.

energy confinement due to damping ($\zeta = 0{\cdot}001$) accounts for the differences between the two measures.

The pass-band width is determined by the coupling ratio ρ [14, 29]. Since ρ is the same for the five systems under consideration they all have the same pass-band width. In this situation, the modal density (the number of modes per unit frequency) is proportional to N and the modes of the larger systems are therefore closer together in frequency. Furthermore, since the damping ratio ζ is the same for all five systems, the larger systems feature greater modal overlap and hence greater energy confinement due to damping.

A striking feature of these results is the dependence on system size. For large values of N (larger than those shown in Figure 9) there would not be significant difference in the behaviour of a system of size $N = m$ and one of size $N = 2m$. This supports the use of the asymptotic localization factor γ for charaterizing the behaviour of large systems. However, Pierre [9] notes that γ should not be used unless N is greater than the 'localization length-scale', γ^{-1}. If this condition is not met, boundary conditions influence the amplitude decay as much as, and perhaps more than, the disorder. Thus, smaller systems are affected more by boundary conditions and are consequently more reverberant. This is evident for

systems of the sizes shown, where the transition to localized behaviour is dependent on N. For example, when $\Upsilon = 1$ (shown as a dotted line in Figure 9), Δ'_{avg} for $N = 3$ is just beginning to increase from its value at $\Upsilon = 0{\cdot}1$, while Δ'_{avg} for $N = 48$ has increased by 50%. It is often recognized that larger systems are more likely to experience localization: Δ'_{avg} provides a quantitative assessment of this effect.

A closer view of the dependence on system size is obtained by considering the quantity,

$$\Lambda = \Delta'_{avg} - \Delta'_{avg}|_{\Upsilon=0}. \tag{32}$$

This is the increase in the total (absolute) energy fraction that remains in an excited subsystem due to imperfection *above that of the perfect system of the same size*. The level of imperfection Υ necessary to achieve a prescribed Λ was calculated as a function of N for $\Lambda = 1, 50, 10, 20\%$ (percentage of the total energy fraction, i.e., 1) and $N = 4, 18, 12, \ldots, 64$. For each N, a least-squares fit for Υ was conducted by calculating Δ'_{avg} (by the Monte Carlo method previously described) at each of the trial values of Υ. The quantity that was minimized was the squared difference between the prescribed Λ and that calculated from equation (32). The results of the calculations are shown in Figure 10.

The obvious observation from Figure 10 is that for a given N, greater imperfection Υ is necessary to achieve larger values of Λ. Of greater interest, however, is that each of the four curves in Figure 10 shows a decrease in Υ needed to achieve a given Λ with increasing system size N. Whilst larger systems are known to be more susceptible to mode localization, this result confirms that they are also more prone to confine broadband energy. Comparing the curve for $\Lambda = 20\%$ to that for $\Lambda = 1\%$ shows that the drop in Υ with increasing N is more pronounced as Λ increases. This unexpected result shows that smaller systems require increasingly greater relative imperfection to achieve the same increase in energy fraction as compared to larger systems.

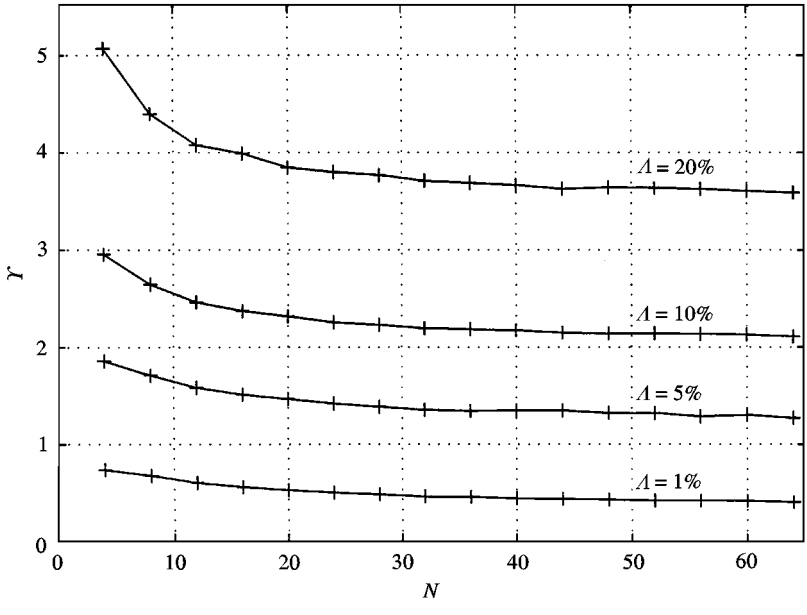

Figure 10. Size dependence: each curve represents the imperfection ratio necessary to increase total energy confinement by Λ.

6. COMPARISON WITH CYCLIC SYSTEMS

The calculations for the linear-chain systems were repeated for their respective cyclic counterparts. All the parameters were the same including the ensembles of imperfection distributions; the only change was the substitution of $[\mathbf{A}_{C,N}]$ for $[\mathbf{A}_{L,N}]$. Results for the cyclic systems are shown in Figure 11.

Unlike linear-chain systems there are significant differences between Δ_{avg} and Δ'_{avg} for cyclic systems at low values of imperfection Υ, especially for small N. This is most evident for $N = 3$, 6, 12 where Δ_{avg} *decreases* slightly with increasing imperfection, reaching a minimum at $\Upsilon \sim 1$, and thereafter rising together with Δ'_{avg}. The cause of this behaviour can be traced to the degeneracy of the eigenstructure of *perfect* cyclic systems. It is well known that all modes except the first mode (and the last mode when N is even) of cyclic systems occur in orthgonal pairs. The modes of each pair have the same natural frequency. When imperfections are introduced into a cyclic system these mode pairs split and each of the modes have a unique natural frequency. However, with small imperfection ratios these natural frequencies are still close in frequency, gradually splitting further apart as the imperfection ratio increases. It was shown in section 4.1 that greater modal overlap leads to greater energy confinement due to damping. What is apparent for $N = 3, 6, 12$ is that energy

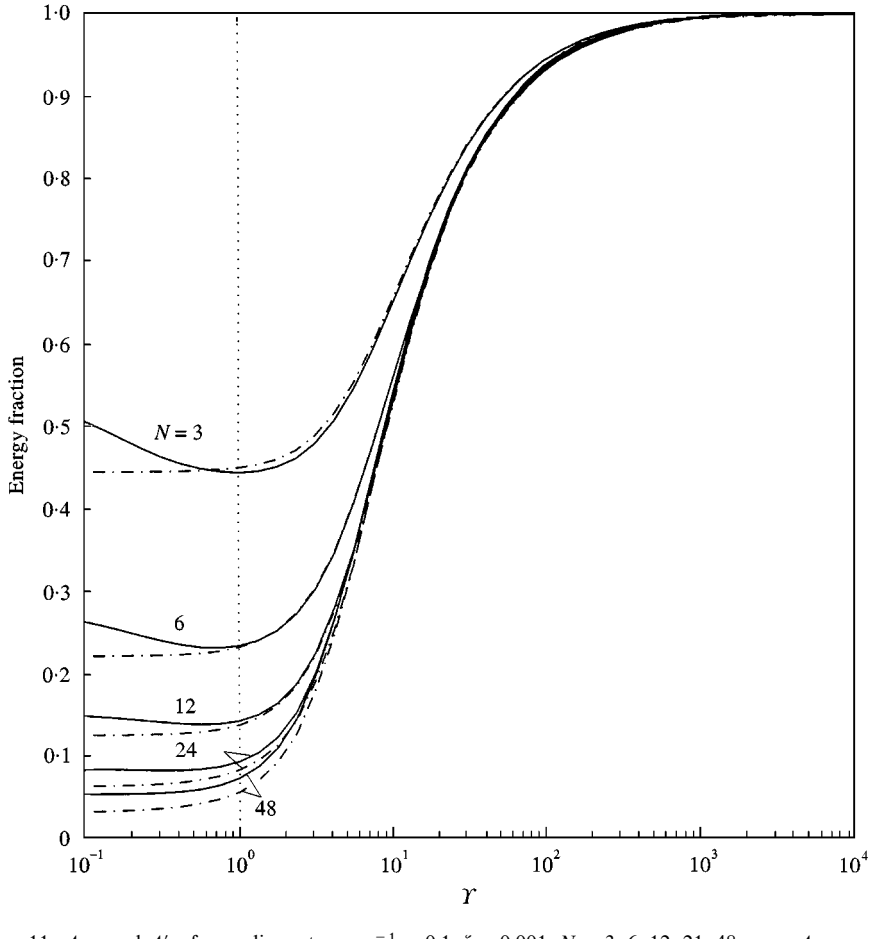

Figure 11. Δ_{avg} and Δ'_{avg} for cyclic systems, $\rho^{-1} = 0{\cdot}1$, $\zeta = 0{\cdot}001$, $N = 3$, 6, 12, 21, 48. —— Δ_{avg}; -·-·- Δ'_{avg}.

confinement due to damping decreases as Υ increases because the modal overlap decreases. This is confirmed by noting the absence of *dips* in Δ'_{avg}, which does not account for energy confinement due to damping.

For $N = 24$ the dip in Δ_{avg} is less noticeable, and it is imperceptible for $N = 48$; indeed, Δ_{avg} for $N = 48$ is indistinguishable, in the main, from its linear-chain counterpart in Figure 11. In part, this insensitivity of larger cyclic systems is due to the increase in modal density with N, which leads to significant modal overlap (and, consequently, energy confinement due to damping) even for *perfect* systems. Thus, the effects of small imperfections will be hidden partly by the higher mean level of modal overlap. Another aspect of the size dependence is explained by considering the result from section 5.4 that larger systems are more susceptible to confining energy (due to imperfections) than smaller systems. Thus, the modes of larger systems are more prone to localize, which means the mode pairs in cyclic systems are more likely to separate as the system size increases. This would diminish energy confinement due to damping and explains the decrease of the dip as N increases from 3 to 48.

To investigate the effect of system size on the energy confinement due to imperfections, Λ (equation (32)) was calculated for cyclic systems over the same parameter range as was used for linear-chain systems shown in Figure 10. The results of these calculations are shown in Figure 12, as are, for comparison, the corresponding results for linear-chain systems. As in the case of linear-chain systems, the imperfection ratio needed to achieve a prescribed Λ in cyclic systems decreases with increasing N. However, the most interesting conclusion from Figure 12 is that cyclic systems are more robust than their linear-chain counterparts. That is, the imperfection ratio must be higher in a cyclic system to achieve the same increase in total energy confinement, than in the corresponding linear-chain system. This is most pronounced for small N, and while the effect diminishes with increasing N, it remains notable even for the largest system in the parameter study ($N = 64$). This is not wholly unexpected and seems physically reasonable. However, to explain the underlying mechanism that causes the relative robustness of cyclic systems it is necessary to investigate the mode shapes: a task undertaken in the next section.

7. MODE SHAPES

In this section the mode shapes of a typical 12 d.o.f. system with both cyclic and linear-chain geometry are investigated. The same imperfections were used in both models. Although only one configuration of imperfections is presented, several configurations were considered and the conclusions presented here are generally valid.

Figure 13(a) shows the modulus of the first eigenvector of a cyclic 12 d.o.f. system with a particular imperfection distribution as Υ increases (i.e., the coupling strength decreases). The data are presented in "plan view" where darker shading indicates greater magnitudes (modal amplitude). It has been shown that the energy fraction rises with increasing Υ. To show this, the corresponding Δ_{avg} curves for the system are overlayed on top of the shaded mode shape.

With small imperfection ratio ($\Upsilon < 1$) the mode shape is still recognizable as the $(1, 1, \ldots, 1)$ mode of the perfect system. As Υ increases, the mode shape sustains greater distortion until a sudden transition occurs at $\Upsilon \approx 7$, whereafter the mode is essentially localized around a single subsystem. For large Υ each of the subsystems is essentially autonomous and the dominant subsystem in each mode follows from the order of the natural frequencies of the uncoupled subsystems. The first mode localizes to the subsystem with the lowest individual natural frequency, the second mode to the subsystem with the next higher intrinsic natural frequency, and so forth.

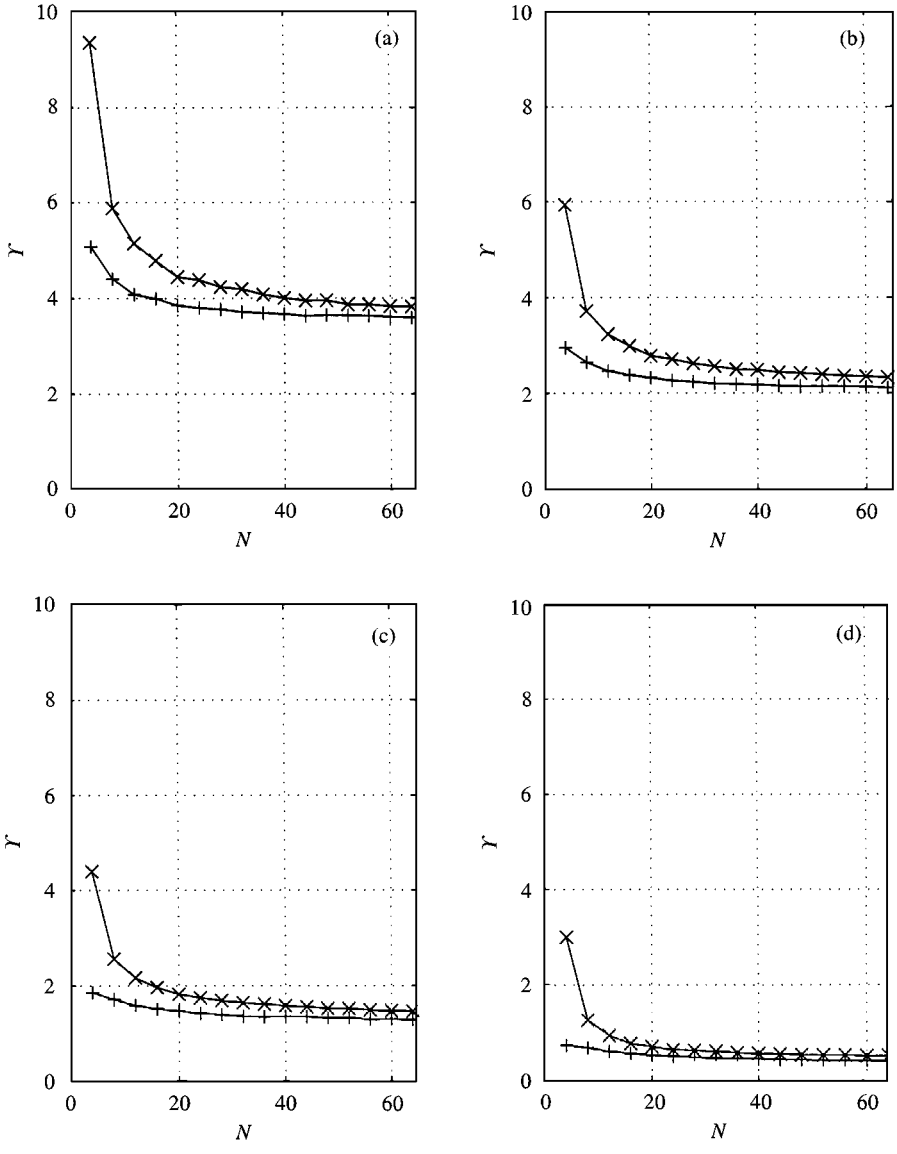

Figure 12. Size dependence: comparison of increase in total energy confinement Λ between cyclic and linear-chain systems: (a) $\Lambda = 20\%$, (b) $\Lambda = 10\%$, (c) $\Lambda = 5\%$, (d) $\Lambda = 1\%$. $\times \times \times$ cyclic; $+ + +$ linear chain.

The sudden transition in Figure 13(a) is marked by a sharp rise in Δ_{avg}. Other local slope discontinuities in the Δ_{avg} curve corresponds to sudden transitions in other modes. However, not all modes experience sudden transitions. Figure 13(b) shows the first mode of the 12 d.o.f. linear-chain system with the same imperfection configuration. Here the mode shape undergoes a smoother transition from periodic behaviour to localized behaviour.

It was observed in preceding sections that appreciable energy confinement due to imperfection occurs only if $\Upsilon > 1$. Examination of the modes themselves shows that this is because significant mode distortion does not occur until $\Upsilon > 1$, a fact that, from Figure 13, holds for both cyclic and linear-chain systems.

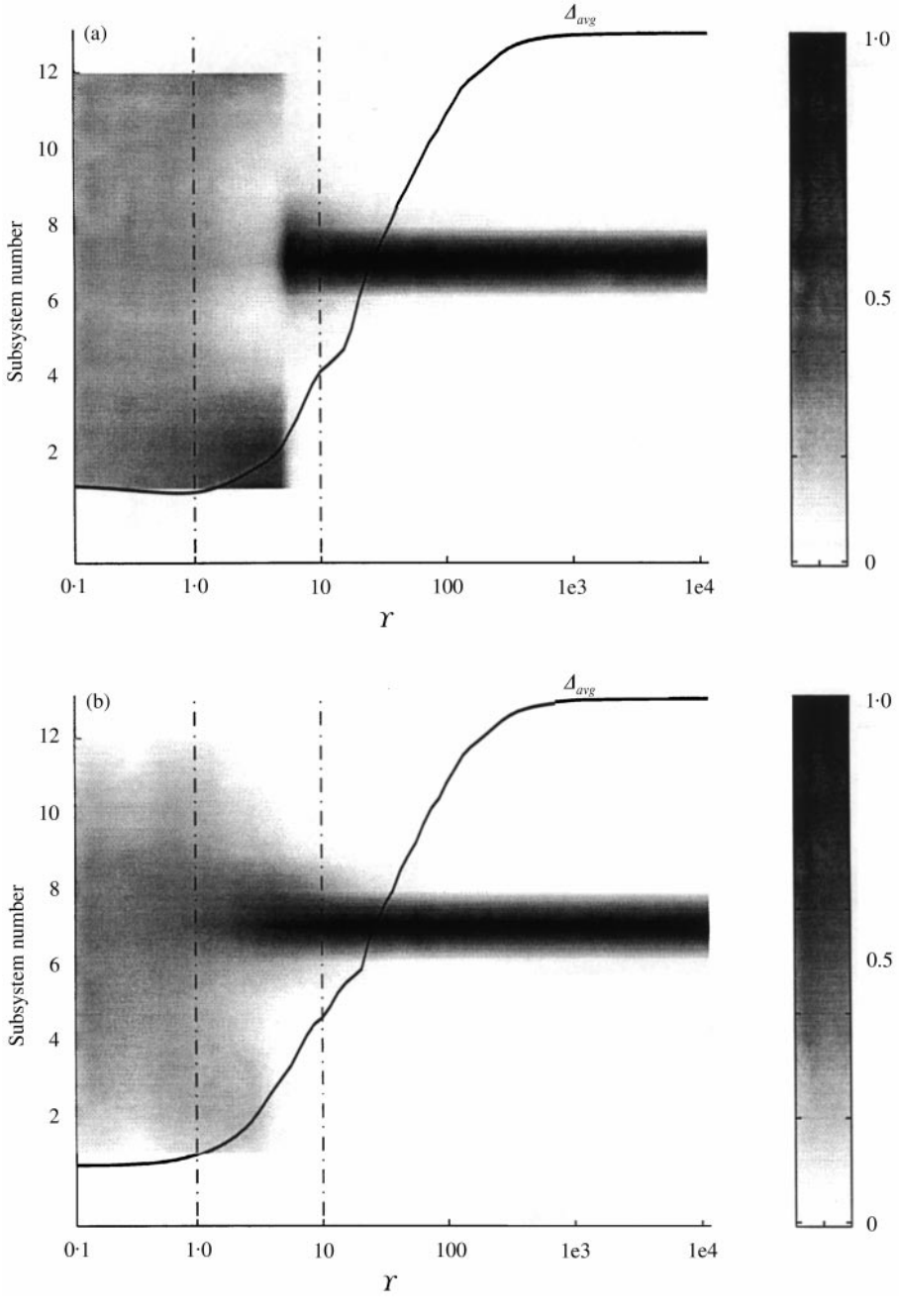

Figure 13. Shaded mode shapes with Δ_{avg} superimposed: (a) cyclic, mode 1, 12 d.o.f. (b) linear-chain, mode 1, 12 d.o.f. system with identical imperfection distribution as cyclic system.

In the preceding section, cyclic systems were shown to be more robust than their linear-chain counterparts. To show why this is, shaded histograms of mode 7 of the cyclic and linear-chain systems are shown in Figure 14. Comparing the cyclic mode shape (Figure 14(a)) to the linear-chain mode shape (Figure 14(b)) for $\Upsilon > 10$ it is apparent that mode 7 of the cyclic system extends over more subsystems than mode 7 of the linear-chain system.

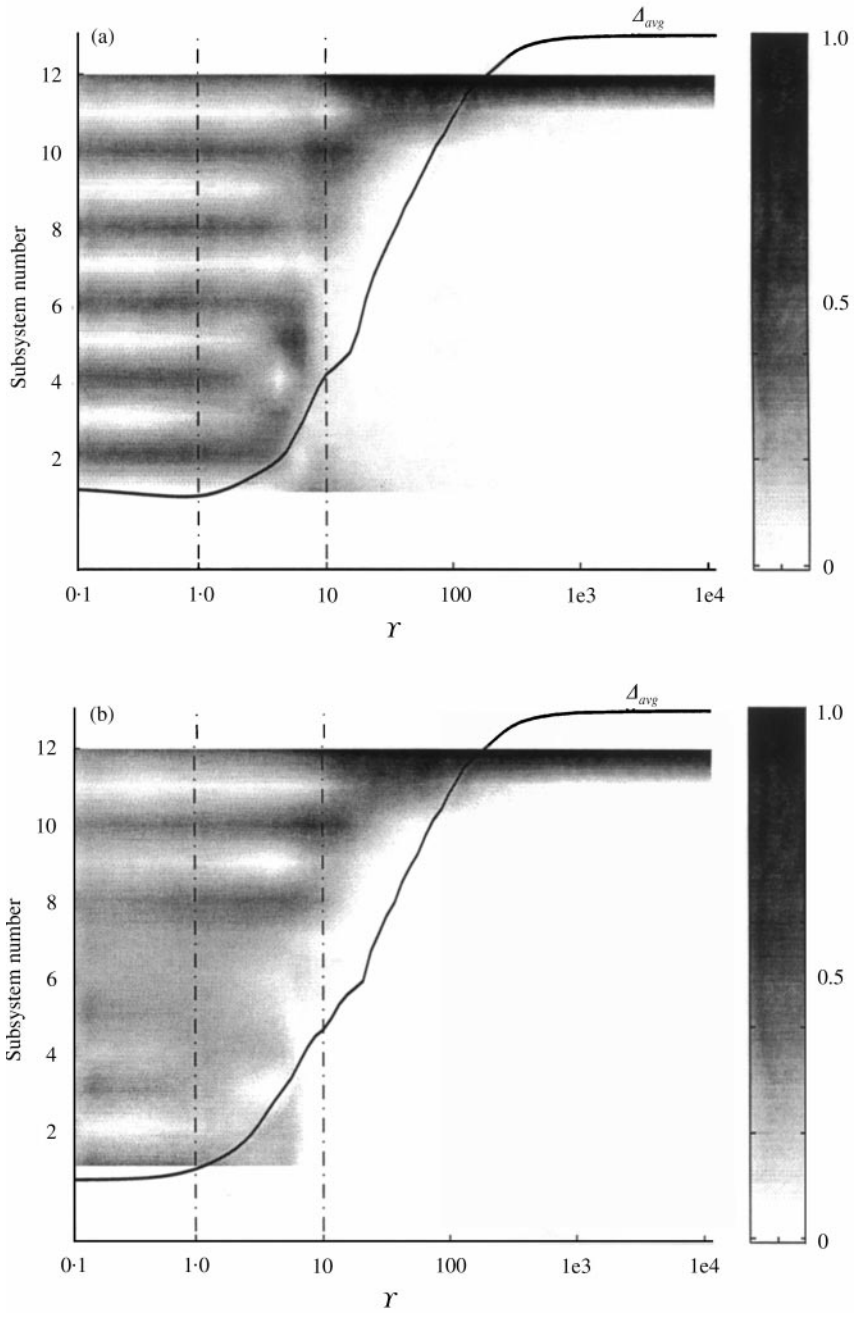

Figure 14. Same as Figure 13 but showing mode 7, which is at the centre of the pass-band. (a) cyclic, mode 7, (b) linear chain, mode 7.

Clearly, this is due to the two *ends* of the cyclic system being connected together, which results in the decay of modal displacements in both directions away from the dominant subsystem (subsystem 12) rather than in just one direction. For $\Upsilon < 10$, Figure 14(a) shows that the cyclic mode shape is more regular and is less prone to distortion than its linear-chain counterpart (Figure 14(b)). In particular, note that the cyclic mode shape

remains similar to that of the perfect system until well into the region $1 < \Upsilon < 10$, whereas the linear-chain modeshape suffers significant distortion before $\Upsilon = 1$. Combined, these two observations lead to the conclusion that the modes of cyclic systems are more robust to imperfections than the modes of linear-chain systems, and that is why the latter are more prone to energy confinement due to imperfections.

8. CONCLUSIONS

Energy confinement in periodic systems has been quantified in terms of the energy fraction, which is based on the response of a system to uniform broadband forcing applied to individual subsystems. The energy fraction Δ_{avg} is formally defined with respect to the subsystem responses, but for light damping Δ'_{avg} (which is nearly three orders of magnitude more economical to calculate) was shown to be an excellent approximation to Δ_{avg}. Δ_{avg} accounts for energy confinement due to imperfection *and* damping, whilst Δ'_{avg} only accounts for energy confinement due to imperfection. This was illustrated with a detailed study of a 2 d.o.f. system, in which it was also shown how energy confinement due to damping increases with the level of modal overlap. A simple result from linear algebra was used to show that the imperfection ratio Υ is *the* parameter governing energy confinement due solely to imperfection. However, energy confinement due to imperfection *and* damping also depends on the coupling ratio ρ, since ρ is a factor in determining the level of modal overlap.

A Monte Carlo study of linear-chain systems showed larger systems to be more vulnerable to energy confinement due to imperfections, but this size effect is less pronounced as system size increases. Repeating the calculations for cyclic systems showed similar size dependence, but more interesting was the observation that cyclic systems are less susceptible than linear-chain systems to energy confinement due to imperfections. An explanation for this was found by comparing the modes of a linear-chain system with those of its cyclic counterpart. This comparison revealed that the modes of cyclic systems are more robust in that, for a given level of imperfection, the modes of cyclic systems extend over a greater number of subsystems.

REFERENCES

1. S.-T. Wei and C. Pierre 1988 *ASME Journal of Vibration, Acoustics, Stress and Reliability in Design* **110**, 429–449. Localization phenomena in mistuned assemblies with cyclic symmetry.
2. D. M. Tang, C. Pierre and E. H. Dowell 1987 *AIAA Journal* **25**, 1249–1257. Localized vibrations of disordered multispan beams: theory and experiment.
3. P. J. Cornwell and O. O. Bendiksen 1989 *AIAA Journal* **27**, 219–226. Localization of vibration in large space reflectors.
4. C. Pierre and P. D. Cha 1989 *AIAA Journal* **27**, 227–241. Strong mode localization in nearly periodic disordered structures.
5. C. Pierre and E. H. Dowell 1987 *Journal of Sound and Vibration* **114**, 549–564. Localization of vibrations by structural irregularity.
6. G. S. Happawana, A. K. Bajaj and O. D. I. Nwokah 1993 *Journal of Sound and Vibration* **160**, 225–242. A singular perturbation analysis of eigenvalue veering and modal sensitivity in perturbed linear periodic systems.
7. H. Matsuda and K. Ishii 1970 *Progress of Theoretical Physics* **45**(suppl.), 56–86. Localization of normal modes and energy transport in the disordered harmonic chain.
8. G. J. Kissel 1987 Technical Report, *AIAA Paper* 87-0819. Localization in disordered periodic structures.

9. C. PIERRE 1990 *Journal of Sound and Vibration* **139**, 111–132. Weak and strong vibration localization in disordered structures: statistical investigation.
10. D BOUZIT and C. PIERRE 1992 *Journal of Vibration and Acoustics, ASME* **114**, 521–530. Vibration confinement phenomenon in disordered, mono-coupled multi-span beams.
11. S.-T. WEI and C. PIERRE 1990 *AIAA Journal* **28**, 861–868. Statistical analysis of the forced response of mistuned cyclic assemblies.
12. D. AFOLABI, O. S. I. NWOKAH and F. M. DAMRA 1990 *Control and Dynamic Systems* **35**, 137–164. On the modal stability of imperfect cyclic systems.
13. P. P. FRIEDMANN, S. D. LUST and O. O. BENDIKSEN 1995 *Journal of Sound and Vibration* **180**, 313–332. Free and forced response of multi-span beams and multi-bay trusses with localized modes.
14. D. YAP 1996 *Ph.D. Thesis, University of Cambridge*. Energy confinement in imperfect periodic systems.
15. O. O. BENDIKSEN 1987 *AIAA Journal* **25**, 1241–1248. Mode localization phenomena in large space structures.
16. G. E. JOHNSON 1989 *Technical Proposal Q*7844/*JPA*/*Issue* 1, *Cambridge Consultants Ltd., Proposal for race to Mars entry*. Design Study for a mars sailcraft.
17. C. H. HODGES and J. WOODHOUSE 1983 *Journal of the Acoustical Society of America* **74**, 894–905. Vibration isolation from irregularity in a nearly periodic structure: theory and experiment.
18. M. E. RAHEB, A. F. VAKAKIS and C. CETINKAYA 1994 *Journal of Sound and Vibration* **172**, 23–46. Free and forced dynamics of a class of periodic elastic systems.
19. C. H. HODGES and J. WOODHOUSE 1989 *Journal of Sound and Vibration* **130**, 253–268. Confinement of vibration by one-dimensional disorder, ii: a numerical experiment on different ensemble averages.
20. E. BALMÈS 1993 *Journal of Sound and Vibration* **161**, 358–363. High modal density, curve veering, localization: a different perspective on the structural response.
21. D. C. HERBERT and R. JONES 1971 *Journal of Physics C*: *Solid State Physics* **4**, 1145–1161.
22. C. H. HODGES 1982 *Journal of Sound and Vibration* **82**, 411–424. Confinement of vibration by structural irregularity.
23. C. H. HODGES and J. WOODHOUSE 1986 *Reports on Progress in Physics* **49**, 107–170. Theories of noise and vibration transmission in complex structures.
24. T. HIROTA 1973 *Progress in Theoretical Physics* **50**, 1240–1247. Degree of localization for the eigenstates in one-dimensional random systems.
25. R. D. PAINTER and W. M. HARTMANN 1976 *Physical Review B* **13**, 479–491. Localization of the vibrational states of binary disordered linear chains.
26. X. M. ZHANG and W. H. ZHANG 1991 *Journal of Sound and Vibration* **151**, 1–7. The reduction of vibrational energy flow in a periodically supported beam.
27. S. NATSIAVAS 1993 *Journal of Sound and Vibration* **165**, 137–147. Mode localisation and frequency veering in a non-conservative mechanical system with dissimilar components.
28. M. P. CASTANIER and C. PIERRE 1993 *Journal of Sound and Vibration* **168**, 479–505. Individual and interactive mechanisms for localisation and dissipation in a mono-coupled nearly-periodic structure.
29. R. S. LANGLEY 1994 *Journal of Sound and Vibration* **178**, 411–428. On the forced response of one-dimensional periodic structures: vibration localization by damping.
30. C. H. HODGES and J. WOODHOUSE 1989 *Journal of Sound and Vibration* **130**, 237–251. Confinement of vibration by one-dimensional disorder, i: theory of ensemble averaging.
31. D. J. EWINS 1984 *Model Testing*: *Theory and Practice*. Research Studies Press Ltd. Letchworth, England.
32. A. W. JOSHI 1984 *Matrices and Tensors in Physics*. Wiley Eastern Ltd, Second edition. New Delhi, India.
33. R. S. LANGLEY 1996 *Journal of Sound and Vibration* **189**, 421–441. The statistics of wave transmission through disordered periodic waveguides.